Magnesium Technology 2013
Edited by: Norbert Hort, Suveen N. Mathaudhu, Neale R. Neelameggham, and Martyn Alderman
TMS (The Minerals, Metals & Materials Society), 2013

GAS-PRESSURE BULGE FORMING OF MG AZ31 SHEET AT 450°C

Alexander J. Carpenter[1], Jon T. Carter[2], Louis G. Hector, Jr.[2], and Eric M. Taleff[3]
[1]Southwest Research Institute; Engineering Dynamics; 6220 Culebra Rd.; San Antonio, TX 78238-5166, USA
[2]General Motors Corp.; Research and Development; MC 480-106-224; 30500 Mound Rd.; Warren, MI 48090-9055, USA
[3]The University of Texas at Austin; Department of Mechanical Engineering; 1 University Station C2200; Austin, TX 78712-0292, USA

Keywords: Magnesium, AZ31, high temperature, bulge forming, grain growth

Abstract

Magnesium (Mg) sheet materials, such as wrought AZ31, possess low densities and high strength- and stiffness-to-weight ratios. These properties suggest that the use of Mg sheet is viable for reducing vehicle weight, an important goal of the automotive industry. Magnesium exhibits poor ductility at room temperature, but high-temperature forming processes may be used to manufacture complex vehicle closure panels. Tensile tests are the most common method of characterizing the plastic deformation of sheet materials. However, gas-pressure bulge tests may be more representative of the stress states that occur during the manufacture of sheet metal components. This study investigates the plastic deformation of AZ31 sheet during both biaxial and plane-strain gas-pressure bulge forming at 450°C. The heights and thicknesses of formed specimens are measured and compared. The deformation behaviors of the AZ31 sheet are related to observations of grain growth and cavitation that occur during forming.

Introduction

The automotive industry is interested in magnesium alloys, such as Mg AZ31 rolled sheet, for potential application in vehicle closure panels [1-6]. The low density of magnesium makes it an attractive material for reducing vehicle mass to increase both fuel efficiency and overall vehicle performance [7-10]. However, wrought Mg alloys exhibit poor ductility at room temperature [11], which is primarily a result of a large disparity between the ease of basal and prismatic slip, coupled with the prevalence of twinning [12-13]. Elevated-temperature forming processes, such as superplastic forming (above 500°C) [14-17] and quick plastic forming (~450°C) [18-20], are required to form currently-available wrought Mg sheet materials into complex automotive components. Gas-pressure bulge tests are useful for characterizing the deformation of sheet materials under these conditions, as the stress states from these tests are characteristic of those that occur during the manufacture of automotive components [21].

At 450°C, AZ31 deforms primarily by grain-boundary-sliding (GBS) creep at slow strain rates and five-power dislocation-climb (DC) creep at fast strain rates [22-24]. For a constant temperature, the strain rate from GBS creep, $\dot{\varepsilon}$, is related to the applied stress, σ, by

$$\dot{\varepsilon} = \frac{A_{GBS}}{d^{p}} \sigma^{n_{GBS}} \quad , \qquad (1)$$

where A_{GBS}, n_{GBS}, and p are material constants, and d is the average grain size of the material [25-26]. As d increases, $\dot{\varepsilon}$ decreases for a constant σ. Thus, the deformation behavior of AZ31 sheet may be strongly affected by both static and dynamic grain growth. Static grain growth during preheating of the AZ31 sheet prior to deformation is thought to slow deformation during GBS creep [23-24]. Similarly, dynamic grain growth during deformation is thought to harden the AZ31 sheet during GBS creep [23]. However, further investigation is needed to link the deformation behavior of AZ31 to microstructure evolution during deformation.

The purpose of this study is to conduct gas-pressure bulge tests of two AZ31 sheet materials with different initial microstructures at 450°C. The deformation behavior of these materials, which is characterized through height and thickness measurements from the formed specimens, is related to grain size and cavitation observations obtained from metallography.

Experimental Procedure

The materials studied were two Mg AZ31 rolled sheet materials each with a thickness of 2 mm. One material was supplied in the H24 temper [27], which results in a partially-recrystallized microstructure. The other material was supplied in the O temper [27], which results in a fully-recrystallized microstructure. The compositions of both materials are provided in Table 1. These AZ31 materials were used in biaxial and plane-strain gas-pressure bulge forming experiments.

Table 1: Mg AZ31 sheet material compositions (wt%) are listed.

Temper	Al	Zn	Mn	Fe	Cu	Ni
H24	3.1	1.0	0.42	0.006	0.003	<0.003
O	3.2	0.77	0.27	0.004	0.003	<0.003
Temper	**Si**	**Ca**	**Be**	**Sr**	**Ce**	**Mg**
H24	<0.1	<0.01	<0.005	<0.005	<0.01	Bal.
O	<0.1	0.0007	<0.005	<0.005	<0.01	Bal.

Biaxial bulge tests were performed using a circular die with an inner diameter of 100 mm. This die shape produces a dome-shaped specimen, as shown in Figure 1(a), that experiences a nearly balanced biaxial stress state at the dome pole during deformation. Plane-strain bulge tests were performed using a rounded rectangular die with dimensions of 254 mm × 51 mm. This die shape results in a tent-shaped specimen, shown in Figure 1(b), that experiences a nearly plane-strain state along much of its length. For plane-strain forming, the rolling direction of the sheet was oriented parallel to the long axis of the forming die. The two halves of each die were contained within an air-circulated furnace which is preheated to 450°C prior to testing.

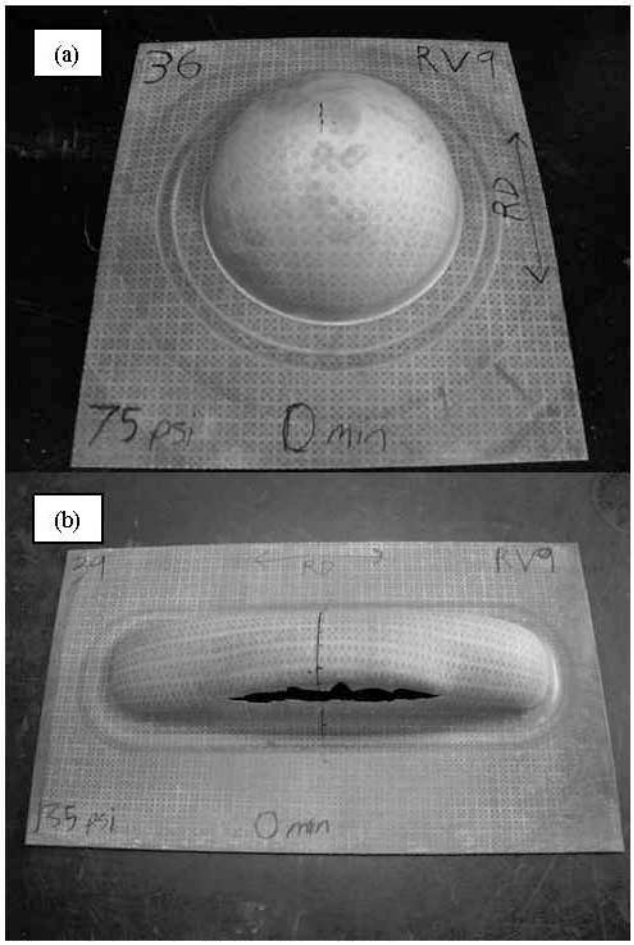

Figure 1: Example (a) biaxial and (b) plane-strain gas-pressure bulge specimens are shown.

Prior to each test, an AZ31 sheet blank sufficiently large to span the sealing beads in the forming dies was placed between the preheated die halves, which were then clamped together to provide a tight seal along the seal bead. Each blank was then preheat soaked for 0, 6, or 11 minutes at 450°C. Upon completion of preheat soaking, gas-pressure was rapidly applied to the lower surface of the blank, causing it to expand into the upper die cavity. The forming pressures used were 520 kPa (75 psi) for biaxial specimens and 930 kPa (135 psi) for plane-strain specimens. These forming pressures were chosen, after numerous experimental trials, to produce an average effective true-strain rate at the specimen pole (for the dome-shaped biaxial specimens) or peak (for the tent-shaped plane-strain specimens) of approximately 10^{-3} s^{-1}. During forming, temperature was monitored with a thermocouple attached to the die and maintained at 450°C. Initial bulge forming experiments were conducted until rupture. For these specimens only, the forming time is the time to rupture. Subsequent experiments were conducted for 1/3rd, 2/3rd, 5/6th and 9/10th of the average rupture time for each material and preheat soak time. Once either rupture or the desired forming time was reached, the specimen was removed from the dies and allowed to cool in air. For biaxial bulge specimens, the dome height and true (thickness) strain were measured at the dome pole. For plane-strain bulge specimens, the height and true strain were measured at the specimen peak. Specimen heights were measured using a stand built specifically for that task, and specimen thicknesses were measured using a magnetic sheet thickness gauge.

Samples for metallographic examination were excised from the gas-pressure bulge specimens to study grain growth and cavitation during deformation. Metallography was performed at locations with effective strains, $\bar{\varepsilon}$, of approximately 0.4, 0.6, 0.8, and 1.2, as calculated from

$$\bar{\varepsilon} = \frac{\sqrt{2}}{3}\left[(\varepsilon_1 - \varepsilon_2)^2 + (\varepsilon_2 - \varepsilon_3)^2 + (\varepsilon_3 - \varepsilon_1)^2\right]^{1/2}, \qquad (2)$$

where ε_i are principal true strains [28]. At each location of interest, the local strain was measured along the longitudinal direction (same as the rolling direction), long-transverse direction (perpendicular to the rolling direction), and short-transverse direction (normal to the sheet) prior to sectioning. Strains normal to the sheet were calculated by measuring the change in thickness due to deformation. Strains within the plane of a sheet were measured with the aid of circle grids imprinted on the sheet prior to deformation. Metallographic specimens were sectioned from the formed bulge specimens at each location of interest and mounted in epoxy. After grinding and polishing, the specimen microstructures were revealed using an acetic-picral etchant (35 mL ethanol, 5 mL H_2O, 5 mL acetic acid, and 2.1 g picric acid). Grain sizes were measured along the rolling, long-transverse, and short-transverse directions using the lineal-intercept method [29]. An average grain size was then calculated by taking the geometric mean of the three directional grain size measurements.

Additional grain-size measurements were obtained from AZ31 sheet specimens annealed in salt. The temperature of the salt bath was maintained at 450°C and monitored using a K-type thermocouple. Specimens were annealed for 80, 360, or 960 s. After annealing was complete, the specimens were quenched in water and prepared for metallography as described in the previous paragraph. The average grain sizes in these specimens were also measured using the lineal-intercept method [29]. The grain sizes from these specimens represent the effects of static grain growth in AZ31 at 450°C.

Results

Height and Thickness Measurements

The specimens shown in Figures 1 exhibit rupture characteristics typical of the biaxial and plane-strain tests. Biaxial bulge specimens always ruptured at the dome pole along a line parallel to the rolling direction. The location of greatest thinning, and the largest strain in these specimens, is near the specimen pole. Rupture occurs as a result of damage accumulated at or near this location of greatest strain, as is shown Figure 1(a). Rupture of plane-strain specimens typically occurred along a line parallel to the specimen long axis and near the line of contact with the die wall. Flow localization occurs preferentially near the line of contact with the die for a plane-strain geometry, particularly when sliding contact is involved. Thus, the greatest specimen thinning was along this line, and rupture occurred here first as a result of damage accumulation. Once a rupture occurs in a plane-strain specimen, it tends to propagate along the line of greatest thinning in the side of the specimen, as is shown Figure 1(b). While rupture of the biaxial specimens does not significantly distort the

specimen shape, rupture of the plane-strain specimens is typically violent enough to cause significant additional deformation. Thus, the final plane-strain specimen height is not representative of the formed height immediately prior to rupture. Because of this, all measurements of height for plane-strain specimens were made from tests halted prior to rupture.

Figure 2 shows the measured (a) dome height and (b) pole true strain for each biaxial specimen as a function of forming time, i.e., elapsed time under gas pressure. The measurements from the ruptured specimens shown in Figure 2 were used to calculate the average inflation rate and pole true strain at rupture for each material and preheat time, and these are provided in Table 2. Average inflation rate is defined as the dome height at rupture divided by the corresponding time to rupture. Table 2 shows that the preheat soak time has an effect on both inflation rate and pole strain at rupture in both materials. The inflation rate of both materials decreased as preheat soaking time increased from 0 to 6 min, though a further increase in preheat soaking time from 6 to 11 minutes had little additional effect on inflation rate. The pole strain at rupture increased as preheat soaking time increased over the range of times tested.

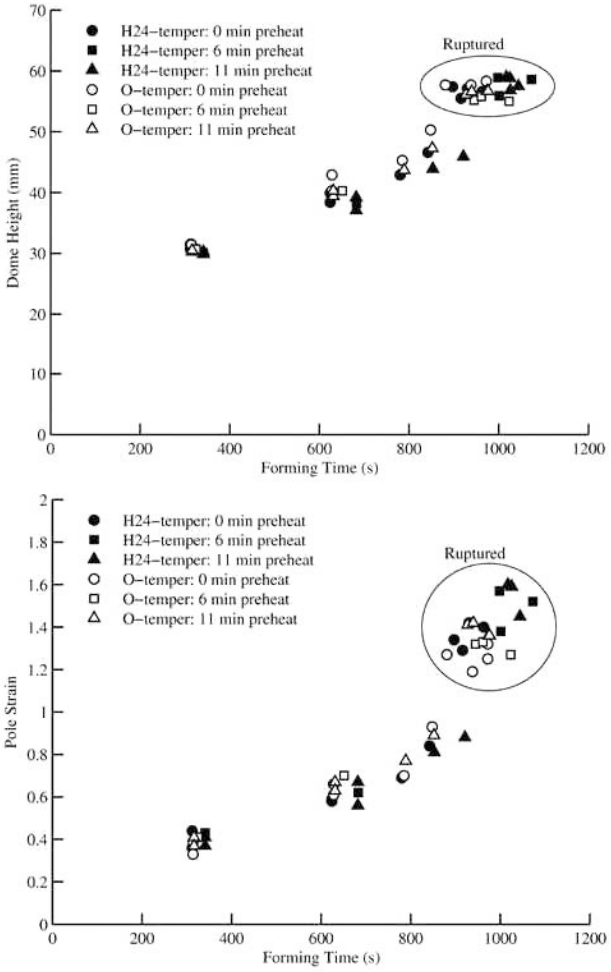

Figure 2: (a) Dome heights and (b) pole true strains are shown as functions of forming time for the gas-pressure biaxial bulge tests. Forming temperature was 450°C and gas pressure was 520 kPa (75 psi) for all tests. The average pole strain rate was approximately 10^{-3} s^{-1}. Specimens tested to rupture are labeled.

Table 2: Average inflation rate and pole strain at rupture are listed for biaxial bulge specimens tested to rupture. The forming temperature was 450°C and gas pressure was 520 kPa (75 psi) for all tests.

Temper	Preheat time (min)	Average inflation rate (mm/min)	Percent difference due to preheat soak
H24	0	3.67	-
	6	3.39	-7.6%
	11	3.39	-7.6%
O	0	3.70	-
	6	3.40	-8.1%
	11	3.55	-4.1%

Temper	Preheat time (min)	Pole strain at rupture	Percent difference due to preheat soak
H24	0	1.36	-
	6	1.49	9.6%
	11	1.56	14.7%
O	0	1.26	-
	6	1.31	4.0%
	11	1.39	10.3%

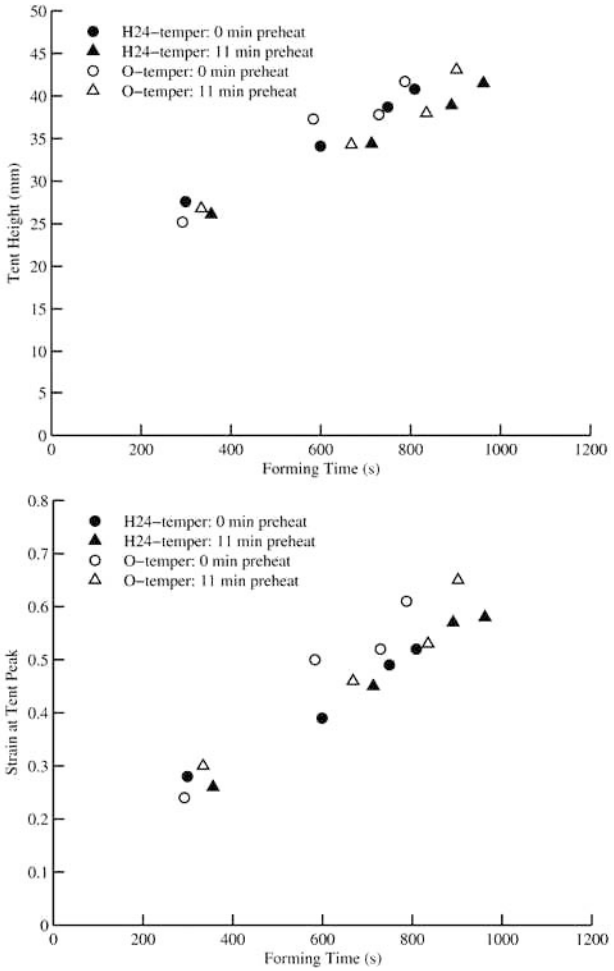

Figure 3: (a) Peak heights (tent heights) and (b) true strains at the peak are shown as a function of forming time for gas-pressure plane-strain bulge tests. Forming temperature was 450°C and gas pressure was 930 kPa (135 psi) for all tests. The average strain rate at the specimen peak was approximately 10^{-3} s^{-1}.

Figure 3 shows the (a) peak height (tent height) and (b) true strain at the peak (top) of plane-strain bulge specimens as a function of forming time. As preheat soak time increases, tent heights tend to decrease slightly for particular forming times. In addition, the peak strain tends to increase more quickly in the O-tempered material than in the H24-tempered material.

Grain Size Measurements

Grain sizes measured in salt-annealed specimens are plotted against annealing time in Figure 4. At an annealing time of 80 s, the grain size of the H24-tempered material is smaller than that of the O-tempered material. However, the grain size of the H24-tempered material grows larger than that of the O-tempered material as annealing time increases. The grain size of the O-tempered material is approximately constant as annealing time increases. The microstructure of the H24-tempered material is clearly less stable at 450°C than that of the O-tempered material.

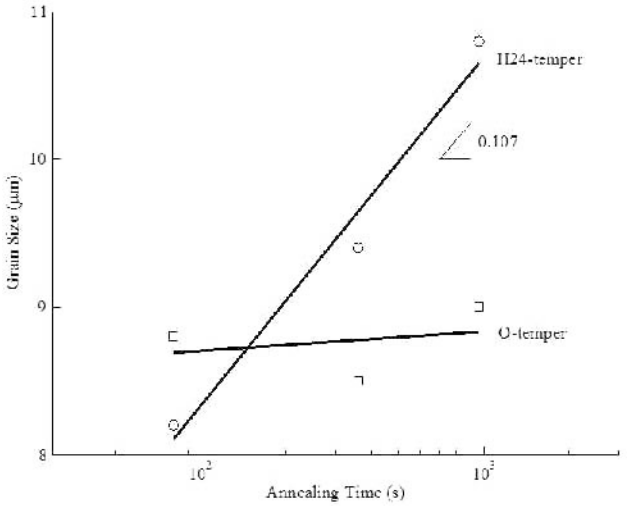

Figure 4: Lineal-intercept grain size measurements of annealed AZ31 specimens are plotted versus annealing time on dual logarithmic scales. Specimens were annealed at 450°C in a salt bath.

Figure 5 presents the average grain size measurements from the H24-tempered bulge specimens plotted against the corresponding effective uniaxial strain at the location of measurement, as calculated through Equation 2, regardless of forming time. Figure 6 presents average grain size measurements from the bulge specimens plotted against forming time, regardless of local strain. The outliers in each figure are from the same specimen and location, which was very close to the location of rupture. These outliers are attributed to recrystallization or abnormal grain growth beyond that from regions of lesser strain. Figure 5 indicates that grain size can be reasonably described as a single-valued function of true strain. However, Figure 6 shows that grain size can vary significantly between different locations with identical preheat soaking times and identical forming times. Thus, grain size is not a single-valued function of forming time. Figures 5 and 6 demonstrate that grain size evolution during forming is better described as a function of strain rather than as a function of time. As true strain increases, grain size increases for $\varepsilon < 0.6$, indicating that the AZ31 sheet materials exhibit dynamic grain growth at these strains. Dynamic grain growth likely causes the strain hardening observed in previous studies [23-24].

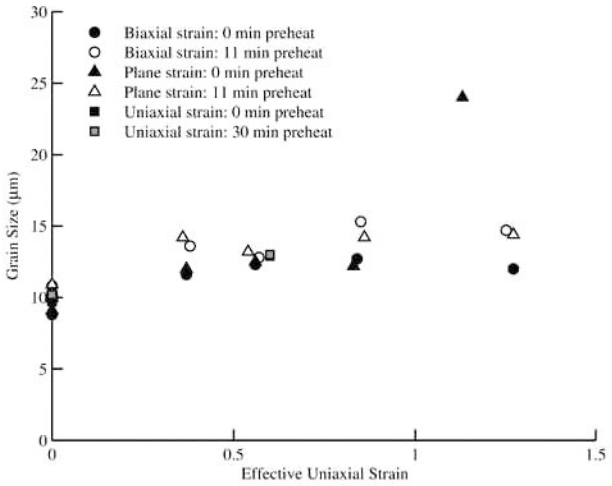

Figure 5: Average lineal-intercept grain size is shown for the H24-tempered material as a function of local effective uniaxial strain. Temperature was 450°C for all specimens.

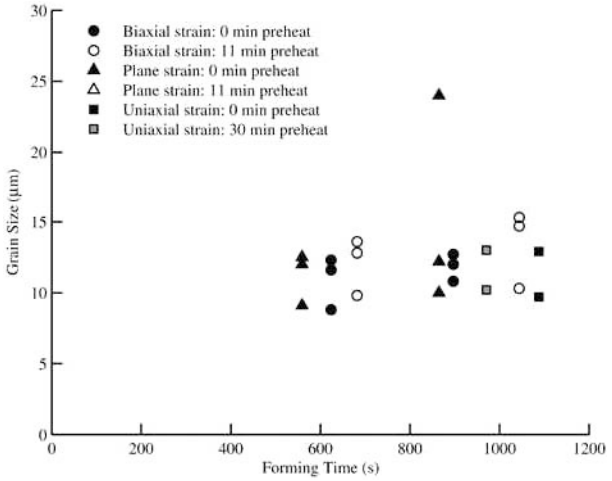

Figure 6: Average lineal-intercept grain size is shown for the H24-tempered material as a function of forming time. Temperature was 450°C for all specimens.

Discussion

The results of this study suggest that the decrease in forming rate during bulge tests as preheat soaking time increases is a result of static grain growth prior to deformation. As grain size increases, the GBS creep rate will decrease according to Equation 1, slowing the deformation rate. The GBS creep rate typically depends on the inverse of grain size to a power of two to three [25-26], making GBS creep rate quite sensitive to even slight grain growth. Figure 4 indicates that the H24-tempered material exhibits static grain growth at 450°C. Thus, this hypothesis reasonably explains why the inflation rate of the H24-tempered material slows as preheat soaking time increases; see Table 2. The data of Table 2 indicate that the inflation rate of the O-tempered material also slows as preheat soaking time increases. This occurs despite minimal static grain growth at 450°C; see Figure 4. Thus, an

additional effect of preheat soaking may exist in the material. Preheat soaking may increase the susceptibility of the O-tempered material to dynamic grain growth in the earliest stages of deformation, and this would produce high initial strain hardening rates that should be observable in experiments. Unfortunately, the available data are not yet sufficient to fully test this hypothesis.

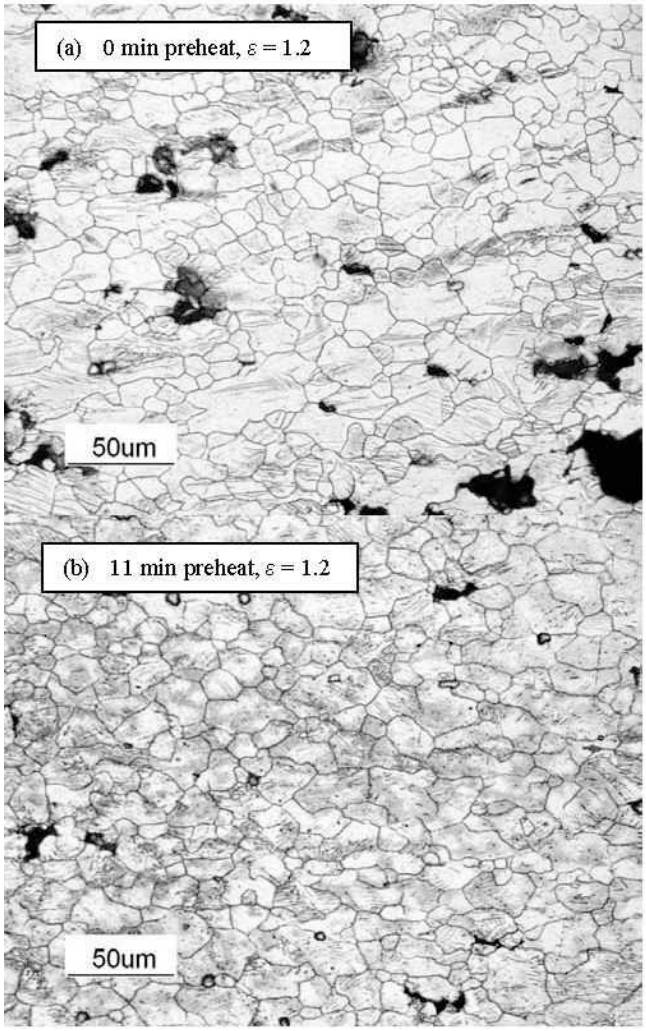

Figure 7: Two photomicrographs from AZ31 H24-tempered biaxial bulge specimens are shown. Both specimens were tested at 450°C and 520 kPa (75 psi). Both photomicrographs are of a region where $\varepsilon = 1.2$ with the rolling direction horizontal and short-transverse direction vertical. Photomicrograph (a) is from a specimen that was not preheat soaked prior to deformation. Photomicrograph (b) is from a specimen that was preheat soaked for 11 minutes prior to deformation. Cavitation damage is clearly less in the preheat soaked specimen.

The increase in pole strain at rupture with preheat soaking time in the biaxial specimens is the result of a reduction in the GBS creep contribution to deformation. Grain growth associated with preheat soaking will reduce the strain rate from GBS creep, thus decreasing the inflation rate; see Table 2. However, Chang *et al.* [30] observed that cavitation develops with strain much more quickly during GBS creep than during solute drag creep in AA5083 sheet, another fine-grained material. If cavitation in AZ31 is also most rapid during GBS creep, this can explain why preheat soaking time increases pole strain at rupture, while decreasing inflation rate. Although pole strain at rupture is increased by a reduction in GBS creep, the dome height is not increased because the greater role of dislocation-climb creep leads to faster localization of thinning at the pole. Figure 7 shows two photomicrographs of material from H24-tempered biaxial bulge specimens tested to an effective strain of 1.2. These photomicrographs show that cavitation does decrease as preheat soaking time increases from 0 to 11 minutes, supporting this theory.

There are two limitations to the grain size data of Figures 5 and 6. First, all of the grain size measurements were made from specimens deformed at approximately 10^{-3} s^{-1}. At this strain rate, both GBS creep and dislocation-climb creep contribute to deformation [22-23]. To separate the effects of GBS creep and dislocation creep on dynamic grain growth, grain size must be measured after deformation at slower strain rates (less than 3×10^{-4} s^{-1}), where GBS creep dominates deformation, and at faster strain rates (greater than 10^{-2} s^{-1}), where dislocation-climb creep dominates deformation [23-23]. Additionally, most of the grain size measurements in Figures 5 and 6 were made at locations of large strain. Further data are required to determine how grain size increases with strain and time at small strains. Note that Figure 5 suggests that strain state has little influence on average grain size. Thus, future studies of dynamic grain growth can be reasonably conducted using a single type of test geometry, such as a simple tensile test.

Conclusions

Gas-pressure bulge tests were conducted using two AZ31 sheet materials at 450°C and pressures selected to maintain true-strain rates of approximately 10^{-3} s^{-1}, and preheat soaking time prior to each test was varied. An increase in preheat soaking decreases the forming rate at a given constant gas pressure. It is proposed that this decrease in forming rate is a result of an increase in grain size caused by the preheat soaking treatment, which produces static grain growth. This increase in grain size decreases the rate of grain-boundary-sliding (GBS) creep, decreasing the forming rate when GBS creep is significant. An increase in preheat soaking time also increases the pole thickness strain prior to rupture in bulge test specimens at 450°C, but does not necessarily increase the maximum dome height achieved. Grain growth from preheat soaking reduces GBS creep, which reduces the rate of cavitation development and allows greater thinning at the dome pole prior to rupture. Dynamic grain growth was observed at 450°C in both biaxial and plane-strain bulge tests. This dynamic grain growth, which is primarily a function of strain rather than time at temperature, is likely responsible for strain hardening at slow strain rates [23], for which GBS creep is significant.

References

1. D. Eliezer, E. Aghion, and F.H. Froes, "Magnesium Science, Technology, and Applications," *Adv. Perform Mater.*, 5 (1998), 201-212.
2. M.M. Avedesian and H. Baker, *Magnesium and Magnesium Alloys* (Novelty, OH: ASM International, 1999), iv.
3. E. Aghion, B. Bronfin, and D. Eliezer, "The Role of the Magnesium Industry in Protecting the Environment," *J. Mater. Process. Tech.*, 117 (2001), 381-385.

4. B.L. Mordike and T. Ebert, "Magnesium: Properties-applications-potential," *Mater. Sci. Eng. A*, 302 (2001), 37-45.
5. M. Easton *et al.*, "Magnesium Alloy Applications in Automotive Structures," *JOM*, 60 (11) (2008), 57-62.
6. M.K. Kulekci, "Magnesium and Its Alloys Applications in Automotive Industry," *Int. J. Adv. Manuf. Technol.*, 39 (2008), 851-865.
7. L.H. Pomeroy, "Advantages of Light-Weight Reciprocating Parts," *Automotive Engineering*, XI (6) (1922), 508-519.
8. G.S. Cole and A.M. Sherman, "Light Weight Materials for Automotive Applications," *Mater. Char.*, 35 (1995), 3-9.
9. A.I. Taub, "Automotive Materials: Technology Trends and Challenges in the 21st Century," *MRS Bulletin*, 31 (2006), 336-343.
10. A.I. Taub *et al.*, "The Evolution of Technology for Materials Processing over the Last 50 Years: The Automotive Example," *JOM*, 59 (2) (2007), 48-57.
11. M.W. Toaz and E.J. Ripling, "Correlation of the Tensile Properties of Pure Magnesium and Four Commercial Alloys with Their Mode of Fracturing," *J. Metals*, 8 (1956), 936-946.
12. J.A. Yasi, L.G. Hector, Jr., and D.R. Trinkle, "First-Principles Data for Solid-Solution Strengthening of Magnesium: From Geometry and Chemistry to Properties," *Acta Mater.*, 58 (2010), 5704-5713.
13. J.A. Yasi, L.G. Hector, Jr., and D.R. Trinkle, "Prediction of Thermal Cross-Slip Stress in Magnesium Alloys from Direct First-Principles Data," *Acta Mater.*, 59 (2011), 5652-5660.
14. G.C. Cornfield and R.H. Johnson, "The Forming of Superplastic Sheet Metal," *Int. J. Mech. Sci.*, 12 (1970), 479-490.
15. A.K. Ghosh and C.H. Hamilton, "Influences of Material Parameters and Microstructure on Superplastic Forming," *Metall. Trans. A*, 13 (1982), 733-743.
16. F.I. Saunders *et al.*, *U.S. Patent 5974847*, 1999.
17. A.J. Barnes, "Superplastic Forming 40 Years and Still Growing," *J. Mater. Eng. Perform.*, 16 (2007), 440-454.
18. M.S. Rashid *et al.*, *U.S. Patent 6253588*, 2001.
19. J.G. Schroth, "General Motors' Quick Plastic Forming Process," *Advances in Superplasticity and Superplastic Forming*, ed. E.M. Taleff *et al.*, (Warrendale, PA: TMS, 2004), 9-20.
20. P.E. Krajewski and J.G. Schroth, "Overview of Quick Plastic Forming Technology," *Mater. Sci. Forum*, 551-552 (2007), 3-12.
21. G. Giuliano and S. Franchitti, "The Determination of Material Parameters from Superplastic Free-Bulging Tests at Constant Pressure," *Int. J. Mach. Tool Manu.*, 48 (2008), 1519-1522.
22. E.M. Taleff *et al.*, "Material Models for Simulation of Superplastic Mg Alloy Sheet Forming," *J. Mater. Eng. Perform.*, 19 (2010), 488-494.
23. P.A. Sherek *et al.*, "The Effects of Strain and Stress State in Hot Forming of Mg AZ31 Sheet," *Magnesium Technology 2012*, ed. S.N. Mathaudhu, (Warrendale, PA: TMS, 2012), 301-306.
24. P.A. Sherek, "Simulation and Experimental Investigation of Hot Gas-Pressure Forming for Light-Alloy Sheet Material" (Master's thesis, The University of Texas at Austin, 2009).
25. O.D. Sherby and P.M. Burke, "Mechanical Behavior of Crystalline Solids at Elevated Temperature," *Progr. Mater. Sci.*, 13 (1968), 325-390.
26. T.G. Nieh, J. Wadsworth, and O.D. Sherby, *Superplasticity in Metals and Ceramics* (Cambridge: Cambridge University Press, 1997), 43-72.
27. ASM International: *Metals Handbook, Vol. 2* (Novelty, OH: ASM International, 2002).
28. J. Hu, Z. Marciniak, and J. Duncan, *Mechanics of Sheet Metal Forming* (Oxford: Butterworth-Heinemann, 2002), 14-27.
29. ASTM E 112-96, *Standard Test Methods for Determining Average Grain Size* (West Conshohocken, PA, ASTM, 1996).
30. J.-K. Chang, E.M. Taleff, and P.E. Krajewski, "The Effect of Microstructure on Cavitation during Hot Deformation of a Fine-Grained Aluminum-Magnesium Alloy as Revealed through Three-Dimensional Characterization," *Metall. Mater. Trans. A*, (40) 2009, 3128-3137.